Energy Conversion and Management 269 (2022) 116145

Contents lists available at ScienceDirect

Energy Conversion and Management

journal homepage: www.elsevier.com/locate/enconman

Effect of natural gas direct injection (NGDI) on the performance and knock behavior of an SI engine

Mahdi Aghahasani [a], Ayat Gharehghani [a,*], Amin Mahmoudzadeh Andwari [b,*], Maciej Mikulski [c], Juho Könnö [b]

[a] School of Mechanical Engineering, Iran University of Science and Technology, Narmak, Tehran, Iran
[b] Machine and Vehicle Design (MVD), Materials and Mechanical Engineering, University of Oulu, P.O. Box 4200, FI-90014 Oulu, Finland
[c] School of Technology and Innovation, Energy Technology, University of Vaasa, Wolffintie 34, FI-65200 Vaasa, Finland

ARTICLE INFO

Keywords:
Numerical modelling
Dual-fuel engine
Natural gas direct injection
Emissions
Knock

ABSTRACT

The unique properties of natural gas (NG), including high availability and lower cost compared with other fossil fuels, make it attractive in internal combustion engine (ICE) application. NG is composed mainly of methane and has greater knock resistance than gasoline, enabling higher compression ratios (CR). In contrast with the distinctive advantages, the NG fueled engines suffer from lower power and torque outputs. To address the subject, this study proposes an approach employing NG direct injection (NGDI) strategy (with higher volumetric efficiency unlike port injection), enabling a higher CR irrespective of knock limit. This work applies reactive computational fluid dynamics (CFD) to investigate spark ignited co-combustion of direct-injected NG with port-admitted gasoline. The results are validated against experimental data. In all simulated cases, the equivalence ratio (i.e., $\varnothing = 1$) and the total input energy are kept constant. Engine performance is evaluated for three CRs (10.5, 11.5, and 12.5:1), five proportion of CNG (R_{CNG}) and at part- and full-load conditions at an engine speed of 1500 rpm. Results indicated that while running $R_{CNG} = 100$ % with a CR of 10.5:1, carbon monoxide (CO) and carbon dioxide (CO_2) emissions were decreased by 29.3 % and 23.5 % respectively, compared to $R_{CNG} = 0$ %. The corresponding emission reduction at CR = 11.5:1 was 27.1 % and 24 %; at CR = 12.5:1 they were 29.6 % and 23.5 % respectively. At each CR, the knock intensity at full load fell significantly as the percentage of NG increased. At a CR of 12.5:1, ringing intensity (RI) at full load decreased by 88.6 % when using $R_{CNG} = 100$ %, instead of $R_{CNG} = 0$ %. Under the same conditions, $R_{CNG} = 25$ % cut RI by 56 %.

1. Introduction

Increasing environmental regulation and restrictions on vehicle emissions make it imperative to adopt new methods to reduce pollution [1,2]. Techniques such as atomization and gasoline mixing mode in spark ignition (SI) engines affect thermal efficiency as well as engine-out emissions [2,3]. Specifically, at stoichiometric conditions, there are local rich regions in the combustion chamber which can lead to more soot emissions [5,6]. Changing the fueling method and using alternative fuels both offer potential to reduce emissions [4,5]. Selection of suitable alternative fuels such as ethanol, methanol, hydrogen and liquefied or compressed NG depends on many factors [8,6]. One of the most important is availability of that fuel in the study area [7,9,12], so NG, which can be produced in different ways, is one of the most suitable alternative fuels for ICEs [13]. Between 1996 and 2016, identified NG reserves have increased by 51.1 %, from 123.5 to 186.6 trillion m^3 [14].

Abbreviations: aBDC, after bottom dead center; aTDC, after top dead center; BSFC, brake specific fuel consumption; bTDC, before top dead center; CD, combustion duration; CAD, crank angle degree; CA50, crank angle where 50 % of heat released; CFD, computational fluid dynamics; CNG, compressed natural gas; CO, carbon monoxide; CO2, carbon dioxide; CR, compression ratio; DI, direct injection; EGR, exhaust gas recirculation; EVO, exhaust valve opening; GDI, gasoline direct injection; GPI, gasoline port injection; H/C, hydrogen/carbon ratio; H2O, water; ICE, Internal combustion engine; IMEP, indicated mean effective pressure; IVC, inlet valve closure; NG, natural gas; NGDI, natural gas direct injection; NO, nitric oxide; NOx, oxides of nitrogen; PFI, port fuel injection; RCNG, proportion of CNG; RI, ringing intensity; RNG, renormalization group theory; RPM, revolutions per minute; SI, spark ignition; SOC, start of combustion; SOI, start of injection; UHC, unburned hydrocarbons.

* Corresponding authors.
E-mail addresses: Ayat_Gharehghani@iust.ac.ir (A. Gharehghani), Amin.Mahmoudzadehandwari@oulu.fi (A. Mahmoudzadeh Andwari).

https://doi.org/10.1016/j.enconman.2022.116145
Received 25 May 2022; Received in revised form 5 August 2022; Accepted 16 August 2022
Available online 23 August 2022

Many studies have been conducted on the parameters affecting combustion in ICEs [12,13] These indicate that the use of alternative fuels [10,11], like hydrogen [19] and NG, instead of conventional liquid fuels, has a great impact on fuel–air mixture formation, combustion quality and emissions [20,21]. Further familiarity with the fuel–air mixing mechanism and combustion method will help ICE manufacturers to optimize their products [22,17].

Many studies have examined the use of alternative fuels considering dual-fuel mode [27] as one of the most effective ways to increase energy savings [28] and reduce emissions from SI engines [23,24]. The most widely studied alternative fuels are alcohols [4,5], hydrogen [29] and NG [30,31]. Those that fuel with excellent characteristics [11,18], perfect technical process and low cost [12], like NG, are considered the most complete alternative fuel for vehicles. As a gaseous fuel, unlike gasoline and other liquid fuels, NG does not need to be atomized and evaporated [34,35], and so suits formation of a homogeneous and complete mixture with air, thus improving combustion efficiency [16,20].

Conventional gasoline engines require fuel additives to prevent knock at full load: these additives rise cost and emissions. However, the high-octane number of NG helps smooth operation and reduces engine knock [14,15], particularly at high load [8,10]. High knock resistance at high load improves combustion efficiency. NG also has acceptable CO_2 reduction potential [36,37] because its hydrogen/carbon (H/C) ratio of 3.8–4.0:1 is significantly higher than gasolinés ~ 1.8:1 [33,38]. Compared with combustion of ordinary gasoline, combustion of NG produces more H_2O than CO_2. Port fuel injection (PFI) fueling systems for NG are already available for light-duty vehicles on the market. However, due to the low power density of NG, its use in PFI competes for air in the intake manifold. This is a disadvantage of using NG in todaýs conventional engines. Furthermore, even if NG is compressed to 250 bar, its volumetric energy density is still only one quarter of gasolinés, thus posing a significant energy storage challenge on the vehicle. Thus, simultaneous use of gasoline and NG [39,25] offers a more appropriate solution for long-distance travel with lower pollution and cost [40,41].

Gas engines with port fuel injection suffer from a reduction in power density at full load due to the displacement of NG with intake air [24,19]. Compared with gasoline direct injection (GDI) performance, a reduction of about 30 % in output torque is observed [32,41]. Recent research using an engine with a special fuel system, including GDI strategy with direct injection of NG, showed best progress at low load [13,22]. Ultimately, NG direct injection (NGDI) has established benefits towards methane slip reduction in low temperature combustion concepts. Recently, Mikulski at al. [42] proven that NG stratification in dual-fuel reactivity controlled compression ignition engine, improves low-load combustion efficiency by as 11 percentage points.

In an SI engine, NGDI can improve the volumetric efficiency of the engine by reducing pumping losses and preventing the fuel from being replaced by inlet air [26]. NGDI injects the fuel after closing the inlet valve, so it does not replace air. Consequently, the volumetric efficiency improves [27,28]. The combustion quality of NGDI engines mainly depends on the quality of the fuel–air mixture. In turn, the formation of the mixture depends on many factors, such as piston crown, type and location of injectors, nozzle geometry, spray pressure, etc. [29,34]. The results of an experimental study on a SI engine equipped with NG and Gasoline showed that at 50 % and 80 % engine throttle position, engine brake power was reduced by 19.25 % and 10.86 %, respectively and in a same manner followed by brake specific fuel consumption (BSFC) reduction by 15.96 % and 14.68 %, respectively when the engine was fueled with CNG compared to that fueled with gasoline [42,45]. Another study concluded that a 25 % reduction in fuel consumption for gasoline and NG co-injection mode compared to only gasoline in a turbocharged SI engine wherein the CR was increased from 9.5:1 to 11.5:1 due to the high octane number of methane while maintaining desired required performance [43]. However, based on the performed research to date, far too little attention has been devoted investigating the influence of direct injection of NG (timing and percentage) on the combustion and emission characteristics (especially knock) of gasoline SI engine representing a NGDI port fuel gasoline (dual fuel) engines. Accordingly, the major objective of this study is to investigate how NG direct injection combined with gasoline port injection fueling system affects the knock phenomenon in the combustion of engine. The effect is investigated numerically for CRs ranging from 10.5:1 to 12.5:1. Engine efficiency, exhaust emissions and combustion characteristics are studied at various R_{CNG} and CRs for part- and full-load conditions. In all studied cases, total input energy is kept constant for each CR. Converge CFD software coupled with Chemkin Solver is employed in the investigation, wherein the numerical results validated against the experimental data for $R_{CNG} = 100$ % and $R_{CNG} = 0$ %. The engine speed chosen for all studied cases is 1500 rpm and combustion considered stoichiometric (equivalence ratio = 1). The rest of the paper is organized as follows: Section 2 explains the details of the numerical model and solver setting for validation of CFD results versus experimental. Section 3 discusses engine performance parameters and emissions along with knock behavior for different CRs and various R_{CNG} at part and full load. The conclusions are drawn in Section 4.

2. Numerical model

Engine combustion and emissions were simulated using the CFD software Converge Studio. Converge needs various settings such as initial condition and input variables to create an appropriate CFD model. This section describes the computational grids and solver settings.

2.1. Computational model, tools and methods

The study uses a single-cylinder engine made by Ford [41], which is representative of a novel gasoline-NGDI fueling system. The engine has two separate fuel systems which can work together. Such a system, with gasoline port fuel injection and side-mounted DI injector for NG, provides high flexibility in engine operation and optimizing performance in different operating conditions. Fig. 1 shows the setup and arrangement of injectors. The DI injector is located between the intake valves at a 60° angle relative to the cylinder axis. This study comprises comparisons of neat gasoline PFI and different R_{CNG}, based on four energy blends of NG: 25 %, 50 %, 75 % and 100 % NGDI. The start of injection (SOI) for NGDI was chosen to be −120 CAD aTDC, so SOI occurs after inlet valve closure (IVC). The test was carried out in part-load mode with a constant engine speed of 1500 rpm. The ambient air pressure and the temperature were equal to 1 atm and 25 °C, respectively. Table 1 summarizes the specifications of the engine.

Close-cycle modelling was used to simulate combustion. So, combustion simulations were performed using Converge Studio v3.0 as a CFD solver from the inlet valve closing (140 CAD bTDC) to exhaust valve opening (150 CAD aTDC). The base grid size is 4 mm and numbers of

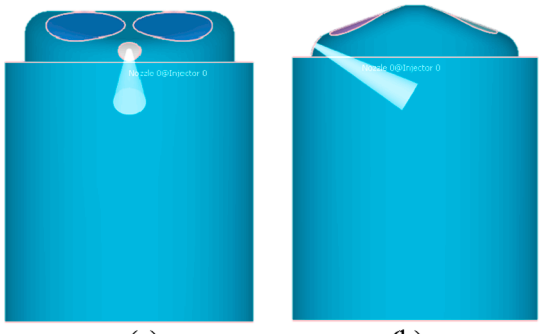

Fig. 1. Modelled geometry imported to Converge Studio (a) left side view; (b) front view.

Table 1
Geometry and operational specifications of the engine.

Parameter	Specification
Displacement [cm^3]	626.4
Stroke [mm]	100.6
Bore [mm]	89.04
Geometric compression ratio	10.5:1
Number of intake/exhaust valves	2/2
Spark plug	NGK, 0.7 mm gap
Exhaust valve open/close [CAD aTDC fired]	150/-350
Intake valve open/close [CAD aTDC fired]	350/-140

adaptive mesh refinement (AMR) were considered for the more sensitive sections. 3 AMR were used to simulate a better distribution of temperature, pressure and CNG with embedding level of 3 for the cylinder region. 2 AMR were used to predict the precise velocity and pressure of CNG injection with embedding level of 3 for the CNG injector. Therefore, the duration of each simulation was increased at the expense of acceptable accuracy. The total number of grids for different piston positions was varied between 600,000–1,700,000. Converge Studio solved conversion of mass, energy and momentum, besides passive and species transport equations during modelling. Converge used the Sage model with set of Chemkin-formatted input files to model combustion. Sage solver modules used Cvodes solver (solves initial value problems for ordinary differential equation systems) to simulate the combustion [44]. Converge used Hiroyasu and Kadota [45] and Zeldovich NO model [46] to simulate emission such as NOx and soot. Atomization of fuel spray droplets was modelled by Kelvin-Helmholtz model (predicts the first break-up of droplets and is based on the wave model) in connection with the Rayleigh-Taylor model (KH-RT). The RT model predicts the future breakup of the droplets and is examined along with the KH model [47].

In the spray modelling, the No Time Counter (NTC) collision model, which involves stochastic (randomly determined) sub-sampling of the parcels within each cell, was used to model droplet collision and coalescence. The NTC collision model employs the direct simulation Monte Carlo method [48].Wall heat transfer affects thermodynamic properties and combustion. Simulation of the heat transfer between wall and turbulent flow needs to consider density and Prandtl number in each step of the solution [48]. Converge Studio generated mesh automatically at each time step of the solution. Embedded sections included liner, head, and piston as boundaries, with spark and nozzle as an embedded region in this modelling.

2.2. Solver setting

Turbulence was modelled using the RNG k-epsilon model. The temperature of cylinder head, cylinder wall and piston surface were set at 450 K. Chemical formulae of NG and gasoline considered CH_4 and IC_8H_{18}, respectively. A skeleton chemical reaction mechanism considering 48 species and 152 reactions, proposed by Liu et al. [49], was used to simulate combustion. In all studied cases, total input energy was kept constant for each CR. As stated, the equivalence ratio for all cases was 1.0. Table 2 provides more details of the test engine operating characteristics during data collection, which were also used to adjust the numerical solver.

Table 2
Engine operational performance.

Parameters	Characteristics
Engine speed	1500 rpm
Equivalence ratio	1.0
Gasoline (E10) LHV(MJ/kg)	42.02
Natural gas (NG) LHV(MJ/kg)	46.93
AFRSTOICH (E10)	14.1
AFRSTOICH (NG)	16.2

2.3. Validation of numerical model

The simulation was performed for low load with an initial pressure of 0.55 bar and an initial temperature of 340 K at IVC and 1500 rpm. The injection duration of NG was 42 CAD, and the SOI was 120 CAD bTDC for all cases. Table 3 lists the measurement instruments. Fig. 2 and Fig. 3 compares the simulation results with experimental data, thus validating the numerical results obtained from the CFD solver. The trends show the variation of in-cylinder pressure and HRR with crank angle. For both 100 % gasoline PFI and 100 % NGDI, the trends of simulation are similar to those of the experiment. For almost all points, the difference between the simulation and experimental in-cylinder pressure is less than 1.5 bar. This equates to less than 1 % for the maximum pressure point.

3. Results and discussion

As well as evaluating different proportions of NG, the numerical simulation also investigated three different CRs. Their combined effects on knock and engine performance for both full- and low-load conditions are discussed here. The results are considered under the following five headings: engine efficiency; thermodynamic properties; combustion characteristics; exhaust emissions; and knock.

3.1. Heat release and efficiency

Indicated mean effective pressure (IMEP) is the basis for evaluating engine efficiency. Engine IMEP is affected by the homogeneity of fuel mixture, so gasoline PFI strategies providing the best homogeneity offer better engine performance. In combined fuel mode, behavior depends upon the R_{CNG}. Fig. 4 shows that for combined fuel mode, the best IMEP for all three CRs is for R_{CNG} = 50 %. IMEP declines with increasing or decreasing R_{CNG}. Additionally, the highest IMEP is related to the CR = 11.5:1. For all ignition modes, ignition timing is selected as that CA50 is placed in the range of 7–9 CAD aTDC and the maximum output torque is obtained. This ignition time was not suitable for maximum efficiency with the CR = 12.5:1, so IMEP was reduced in this case. As shown in Fig. 5, the highest flame propagation speed happened in R_{CNG} = 0 % (i.e., only gasoline). As R_{CNG} increases (especially above R_{CNG} = 50 %) the flame propagation speed and as a result the combustion speed decreases. The higher combustion speed leads to constant volume combustion (ideal combustion for Otto cycle), which improves the thermal efficiency and IMEP. Further increasing in R_{CNG} value will drop the combustion speed leading to lower IMEP. Ze Liu et al. [51]pointed out that in gasoline port injection plus NG gas direct injection (GPI + NGDI) mode of operation, the increasing of NG prpportion by more than 30 % the IMEP dropped drastically.

Tables 4 and 5 list engine outputs such as gross work and total in-cylinder heat release for part- and full-load conditions. The reduction of gross work and total heat release in the combined fuel mode compared to the R_{CNG} = 0 % is apparent. The maximum amount of gross work in the combined fuel and part-load mode is achieved with R_{CNG} = 50 %. Fig. 4 shows the effect of R_{CNG} on gross work (J), total heat release (J), and IMEP. The highest total heat release occurs for the R_{CNG} = 50 % at a CR = 10.5:1, while the highest gross work rate is for the R_{CNG} = 0 %. The main reason for high gross work in the case of R_{CNG} = 0 % is the early injection of gasoline (-540 CAD aTDC), thus creating better

Table 3
Measurement instruments.

Apparatus	Production type
Ignition and injection timing	Motec M800
Throttling regulators	Parker Pilot
Fuel flows	Coriolis fuel meter CMF010
Crank angle position	AVL 365X
In-cylinder pressure	AVL GU21C

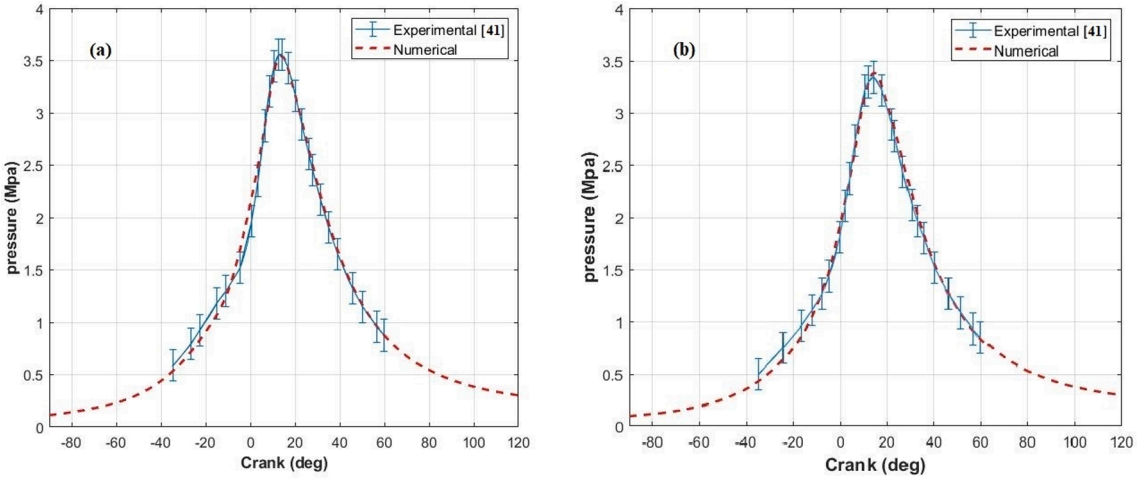

Fig. 2. Pressure trace validation (a) 100 % gasoline PFI; (b) 100 % CNG DI (Experimental data adapted from M. Pamminger et al. [41]).

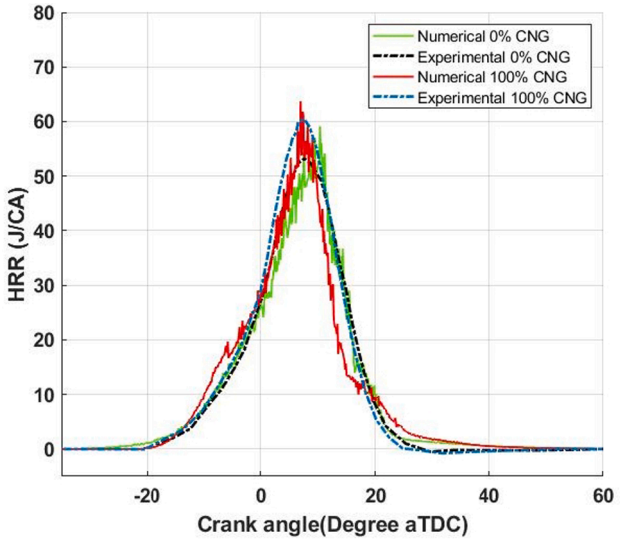

Fig. 3. Heat release rate trace validation for 100 % gasoline PFI and 100 % CNG DI (Experimental data adapted from M. Pamminger et al. [41]).

mixture distribution. Although $R_{CNG} = 50$ % shows the best performance in combined fuel mode at part load, at full load, $R_{CNG} = 100$ % shows better heat-release performance.

3.2. Thermodynamic properties

Temperature and pressure inside the cylinder are the important thermodynamic properties discussed in this section. Fig. 6 shows changes of in-cylinder pressure at part load and with CR = 10.5:1 when using different percentages of CNG. At −35 CAD aTDC, while combustion has not yet begun, the pressure increases with addition CNG. The main reason is direct injection of CNG after closing the air inlet valve, which improves the volumetric efficiency. That is one of the main advantages of direct injection of CNG. As shown in Fig. 6, the highest peak pressure is with $R_{CNG} = 100$ % (36 bar) and the lowest peak pressure is with $R_{CNG} = 0$ % (34.06 bar). However, note that contrary to expectations, $R_{CNG} = 50$ % displays a higher peak pressure than $R_{CNG} = 75$ %. This reversal of the general trend could be due to the dominance of the effect of higher combustion speed of gasoline fuel for $R_{CNG} = 50$ % mode. This effect may be overcoming the higher amount of pressure inside the cylinder before combustion with $R_{CNG} = 75$ %.

Fig. 7 also shows the changes of in-cylinder pressure at part load for different R_{CNG}, but with CRs of 12.5:1 and 11.5:1. The volume of the combustion chamber at TDC is equal for all three CRs. As the CR increases, the peak pressure grows for all fuel combinations. However, the

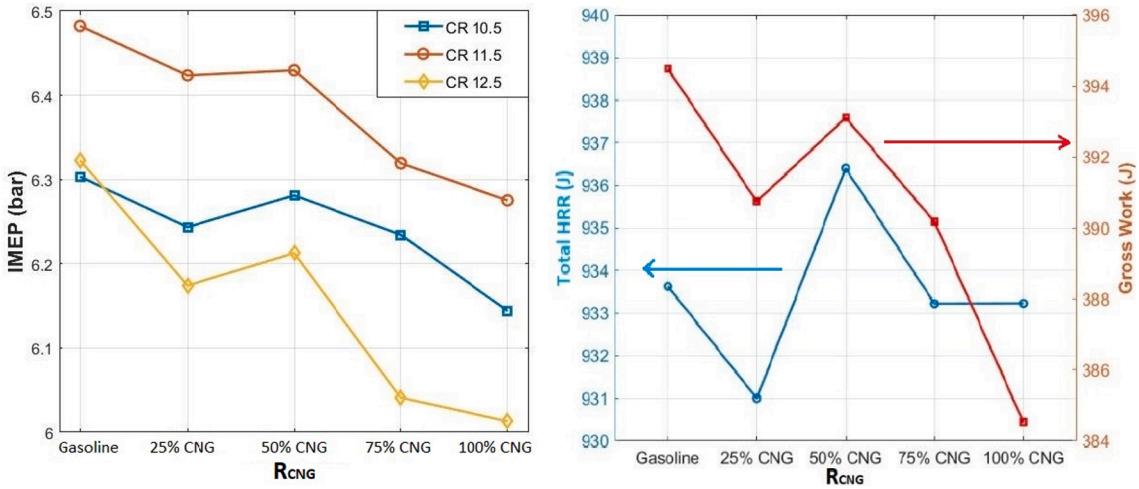

Fig. 4. IMEP, total heat release and gross work for various case studies.

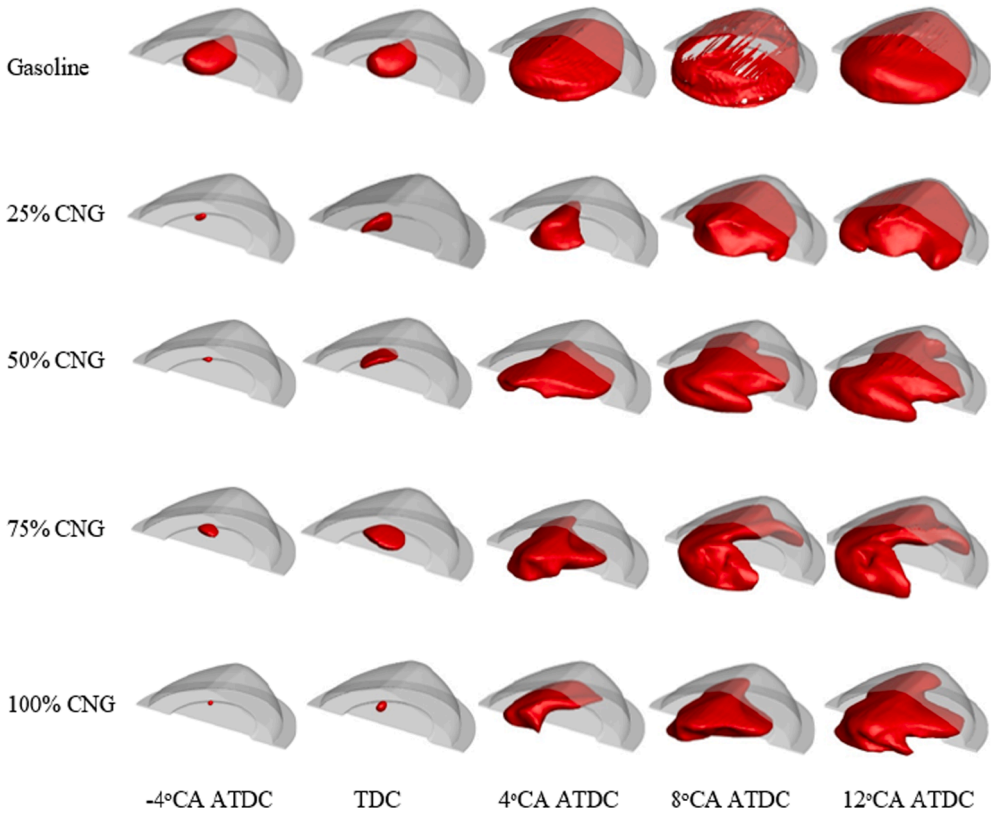

Fig. 5. Contours of flame propagation for various case studies at full load and CR 12.5:1.

Table 4
Engine output characteristics of each case study for part load.

Compression Ratio	Case	Gross Work (J)	Total Heat Release (J)	IMEP (bar)
CR 10.5:1	Gasoline	394.5	933.6	6.30
	0.25 CNG	390.7	931.0	6.24
	0.50 CNG	393.1	936.4	6.28
	0.75 CNG	390.2	933.2	6.23
	1.00 CNG	384.5	933.2	6.14
CR 11.5:1	Gasoline	448.4	1021.5	6.48
	0.25 CNG	444.4	1024.3	6.42
	0.50 CNG	444.8	1028.5	6.43
	0.75 CNG	437.2	1027.9	6.32
	1.00 CNG	434.1	1023.6	6.28
CR 12.5:1	Gasoline	479.1	1113.0	6.32
	0.25 CNG	467.8	1115.9	6.17
	0.50 CNG	470.7	1120.5	6.21
	0.75 CNG	457.7	1121.5	6.04
	1.00 CNG	455.6	1116.7	6.01

Table 5
Engine output characteristics of each case study for full load.

Compression Ratio	Case	Gross Work (J)	Total Heat Release (J)	IMEP (bar)
CR 10.5:1	Gasoline	784.5	1802.6	12.54
	0.25 CNG	777.8	1800	12.43
	0.50 CNG	761.54	1792.5	12.17
	0.75 CNG	767.78	1798	12.27
	1.00 CNG	764.47	1800.7	12.21
CR 11.5:1	Gasoline	890.33	1979	12.87
	0.25 CNG	880.85	1979.6	12.73
	0.50 CNG	863.34	1974.5	12.73
	0.75 CNG	867.26	1973.5	12.54
	1.00 CNG	862.2	1978	12.46
CR 12.5:1	Gasoline	962.85	2156	12.71
	0.25 CNG	941.85	2145	12.43
	0.50 CNG	913.14	2130	12.60
	0.75 CNG	933.08	2155.9	12.31
	1.00 CNG	927.87	2157.5	12.25

maximum pressure with 100 % gasoline fuel, which was in fifth place for CR = 10.5:1, rises to second for CR = 11.5:1 and to first place with CR = 12.5:1. This primarily is due to the fact that the increase in CR raises the temperature of the combustion chamber. This accelerates the combustion rate for $R_{CNG} = 0$ % because gasoline ignites at a lower temperature (340 °C) than NG (540 °C).

Another reason for this is that the fuel–air mixture for $R_{CNG} = 0$ % has lower specific heat than in the combined gasoline-NG mode: this causes the fuel–air mixture temperature to rise faster, resulting in faster combustion. Of course, this rapid rise in peak pressure with pure gasoline

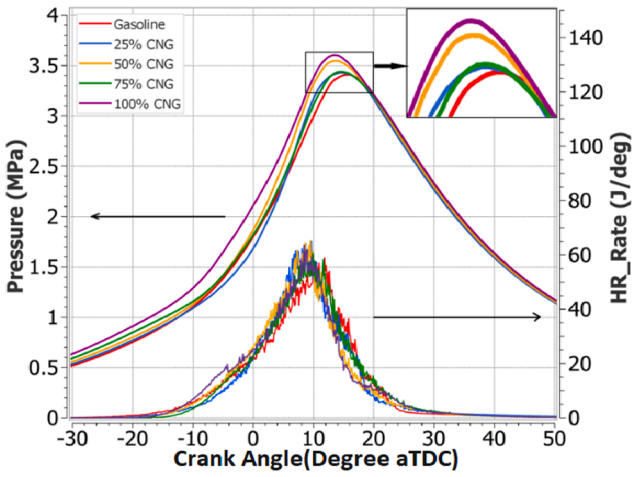

Fig. 6. Comparison of pressure vs crank angle for different R_{CNG} and CR = 10.5:1.

also increases the likelihood of engine knock, especially at full load. This is discussed in detail in Section 3.5. Tables 6 and 7 show maximum in-cylinder pressures and temperatures at part load and full load respectively.

3.3. Combustion characteristics

The study investigated three key combustion characteristics: start of combustion (SOC); crank angle degree where 50 % of fuel burned (CA50); and combustion duration (CD). Ignition timing for all cases was adjusted to obtain maximum output torque. According to studies in this field, under full load at low speeds, GDI performance is limited due to knock, and so therefore the CA50 position should be 20–30 CAD aTDC. But with gasoline PFI and NGDI, the optimal ignition time is when the CA50 is 7–9 CAD aTDC [25,23]. Therefore, it can be said that all the studied cases lead to the maximum output torque of the engine. Fig. 8 shows the SOC and CD for all three CRs with different R_{CNG} at part load. As can be seen, first the SOC is retarded by increasing the R_{CNG}, then advanced. 25 % of NG has the longest delay among the other cases.

Tables 8 and 9 show combustion characteristics of each case study at part load and full load respectively. It should be noted that combustion duration was calculated from the difference between CA90 (crank angle degree where 90 % of fuels burned) and CA10 (angle where 10 % fuels burned). Fig. 8 depicts these approximate values of combustion duration.

As can be seen at both load points, the shortest combustion duration is with R_{CNG} = 0 % and CR = 12.5:1. This mainly is due to the high combustion speed of gasoline compared to NG, and also because of gasolinés low auto-ignition temperature. In the combined gasoline/CNG mode, the greatest reduction in combustion duration as CR increases is for the R_{CNG} = 50 %.

3.4. Exhaust emissions

Fig. 9 shows the mole fractions of CO and CO_2 at the moment of exhaust valve opening (EVO) for the three different CRs and all five fuel combinations at part load. As can be seen, as CR rises, CO pollutants in the combined fuel modes decrease slightly, but CO_2 increases slightly. Both outcomes in response to the increase of the CR in the combined fuel modes stem from the higher temperature of the combustion chamber in the higher CRs, resulting in more complete combustion. On the other hand, Fig. 9 also shows that increasing R_{CNG} leads to a significant reduction in CO and CO_2. This is because methane has the lowest carbon to hydrogen ratio among fossil fuels. At CR = 10.5, the amounts of CO and CO_2 for the R_{CNG} = 100 % are lower by 29 % and 23.5 % respectively than with R_{CNG} = 0 %. Ze Liu et al. [51] pointed out that the gasoline port injection plus NG direct injection (GPI + NGDI) mode has a positive effect on CO reduction. They pointed out that, 120°bTDC of NG direct injection timing minimises CO emissions. The GPI + NGDI mode under this condition reduces CO by 47.5 % on average compared with the pure gasoline data.

Fig. 10 illustrates the amount of NOx at the moment of EVO for all three CRs and all five fuel compounds at part load. It is apparent that an increase in CR leads to a reduction in NOx for all fuel compounds. Because combustion in all cases was stoichiometric, the amount of mole fraction-O_2 in the combustion chamber after combustion is very low (on a scale of 10^{-8}). On the other hand, as shown in the Fig. 9, a higher CR and the consequential rising engine temperature means combustion is more complete, resulting in increased carbon dioxide. This reduces the oxygen in the combustion chamber available to react with nitrogen, and hence less NOx forms at high CRs.

Fig. 10 shows that increasing the R_{CNG} from 25 % to 100 % leads to a reduction in NOx. This is a consequence of a reduction in the maximum temperature of the combustion chamber. The mixture's specific heat capacity rises as the R_{CNG} increases, and since the total energy released for all fuel compounds is approximately equal, the rate of temperature rise diminishes with increasing R_{CNG}, thus reducing the amount of NOx. Table 10 shows the amount of unburned hydrocarbons (UHC) pollutant at the moment of EVO (-150 CAD aTDC) for all three CRs and the five fuel compounds. It can be seen that the amount of UHC is on the same scale for the 10.5:1 and 11.5:1 CRs, but the amount of UHC growth sharply when raising the CR to 12.5:1. This highest CR entails a greater displacement course, so the piston is in a lower position than in the

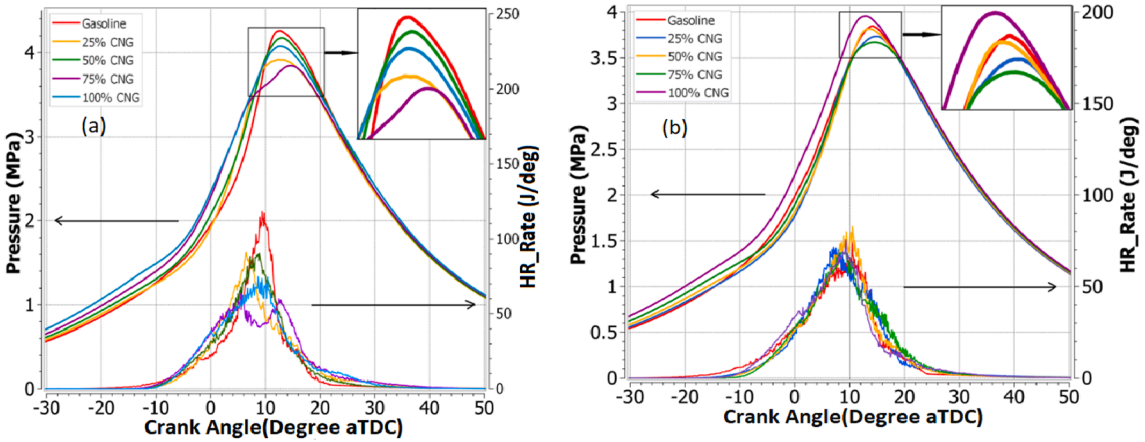

Fig. 7. Comparison of pressure vs crank angle for different R_{CNG}. (a) CR = 12.5:1; (b) CR = 11.5:1.

Table 6
Maximum in-cylinder temperature and pressure (part load).

Compression Ratio	Case	EVO Pressure (bar)	Max. Pressure (bar)/ CAD aTDC	EVO Temp. (K)	Max. Temp. (K)/ CAD aTDC
CR 10.5:1	Gasoline	2.44	34.1/15.9	1451.2	2570.9/ 21.3
	0.25 CNG	2.45	34.3/14.8	1439.8	2514.8/ 18.8
	0.50 CNG	2.47	35.5/14.5	1440.7	2508.0/ 19.9
	0.75 CNG	2.50	34.4/14.5	1441.7	2488.2/ 21.6
	1.00 CNG	2.50	36.0/13.6	1423.7	2473.0/ 20.8
CR 11.5:1	Gasoline	2.41	38.4/14.1	1430.5	2577.5/ 19.5
	0.25 CNG	2.42	37.3/15	1423.1	2527.4/ 16.6
	0.50 CNG	2.41	38.1/13.6	1429.6	2525.9/20
	0.75 CNG	2.40	36.7/14.3	1410.0	2495.0/21
	1.00 CNG	2.48	39.5/12.9	1413.5	2479.4/ 19.7
CR 12.5:1	Gasoline	2.16	42.6/12.7	1284.6	2600.9/ 17.4
	0.25 CNG	2.16	39.1/12.4	1271.6	2440.0/ 19.3
	0.50 CNG	2.19	41.8/13	1273.4	2511.2/ 17.6
	0.75 CNG	2.21	38.4/14.6	1270.9	2403.0/ 19.8
	1.00 CNG	2.24	40.8/12.7	1274.0	2418.0/ 18.5

Table 7
Maximum in-cylinder temperature and pressure (full load).

Compression Ratio	Case	EVO Pressure (bar)	Max. Pressure (bar)/ CAD aTDC	EVO Temp. (K)	Max. Temp. (K)/ CAD aTDC
CR 10.5:1	Gasoline	4.82	76.3/12.4	1481.4	2685.1/ 15.1
	0.25 CNG	4.88	75.88/11.2	1486	2596.4/ 14.4
	0.50 CNG	4.91	70.57/13.2	1477.2	2495.8/ 17
	0.75 CNG	4.93	72.88/11.4	1465.6	2500.1/ 17.1
	1.00 CNG	4.92	71.1/12.9	1448.8	2484.6/ 19.8
CR 11.5:1	Gasoline	4.75	84.9/10.6	1458.1	2688.1/ 14.3
	0.25 CNG	4.78	84.5/10.5	1456	2630.5/ 13.9
	0.50 CNG	4.83	80/12	1453.9	2537.9/ 14.9
	0.75 CNG	4.83	80.6/11.4	1436	2546.2/ 16.7
	1.00 CNG	4.88	75.412.1	1435	2469.9/ 19.5
CR 12.5:1	Gasoline	4.36	95.1/9.4	1337.8	2712.5/ 12
	0.25 CNG	4.41	90.5/10.7	1339.5	2620.4/ 13.7
	0.50 CNG	4.43	83.3/10.9	1332.3	2439.8/ 16.2
	0.75 CNG	4.42	87.8/10.4	1313.3	2531.9/ 16.1
	1.00 CNG	4.45	85.2/11.4	1308.6	2471.6/ 16.1

engine's initial state (CR = 10.5:1). Because the fuel injection angle is constant, when the piston surface is lower it is less able to create tumble in the fuel–air mixture. As a result, the mixing quality suffers and inhomogeneity is created in the combustion chamber, leading to incomplete combustion and more UHC.

Fig. 12 shows how CO, CO_2, NOx, soot and temperature are distributed for a CR of 10.5:1 at 18 CAD aTDC. It is immediately apparent that CO, CO_2 and temperature are highest for $R_{CNG} = 0$ %, and their values decline as the R_{CNG} increases. Conversely, as shown in Fig. 11 soot rises with the R_{CNG} percentage. One of the main causes of this soot formation is poor fuel mixing during stratified charging [36,37]. It should be borne in mind that the engine is not designed primarily for direct fuel injection, so is not well-suited for mixing fuel and air with this type of injection. And because SOI started from −120 CAD aTDC, there is not enough time to create a homogeneous mixture, resulting in soot formation.

It is evident from Fig. 12 that the amount of CO and CO_2 declines as R_{CNG} increases, but there is also a clear inhomogeneity in the distribution of pollutants at $R_{CNG} = 25$ %. This inhomogeneity lessens significantly as R_{CNG} rises. To better understand this, Fig. 13 depicts the equivalence ratio distributions for 25 % and 100 % CNG, at 10 CAD after SOI. The amount of fuel penetration, and consequently tumble created in the combustion chamber, is greater with $R_{CNG} = 100$ %, due to higher injection pressure and the higher momentum of NG. This improves mixing in the combustion chamber, resulting in a more homogeneous distribution of CO and CO_2 when $R_{CNG} = 100$ %.

3.5. Knock investigation

Increasing the CR in ICEs improves efficiency. Equation (1) is the mathematical basis of this principle. From Equation (1) it can be perceived that the Otto cycle efficiency depends directly upon the CR, wherein K for combustion products of the fuel/air mixture is often considered at approximately 1.3. T_3 and T_1 are equivalent to T_{max} and T_{min}, respectively. V_2 and V_1 are the cylinder volume at TDC and BDC, respectively. This equation explains why raising the CR increases Otto cycle efficiency [50,52]:

$$\eta_{th} = 1 - \frac{T_4 - T_1}{T_3 - T_2} \rightarrow \eta_{Otto} = 1 - \left(\frac{V_2}{V_1}\right)^{K-1} = 1 - \frac{1}{CR^{K-1}} \quad (1)$$

Consequently, the use of higher CRs to improves thermal efficiency and allow reduction in engine size is highly regarded by engineers. However, the increased probability of knocking in the engine limits the ability to raise CRs. Knocking damages the engine, increases noise and reduces thermal efficiency. Various methods have been proposed to reduce the possibility of knock, including the use of exhaust gas recirculation (EGR), lowering the equivalence ratio, reducing the inlet air temperature and using fuels with better knock resistance properties [51,54]. NG has a higher-octane value and higher auto-ignition temperature than gasoline, underpinning CNGs potential as a knock-reducing fuel that paves the way for higher CRs and thus greater efficiency. An important method for evaluating knock in ICEs is to measure ringing intensity (RI). Equation (2) has been introduced by Eng [55] for RI to indicate the tendency for engine knock. The RI (MW/m^2) is a measure that correlates with the acoustic energy of the resonating pressure wave:

$$RI \approx \frac{1}{2\gamma} \bullet \frac{\left(\beta \bullet \left(\frac{dP}{dt}\right)_{max}\right)^2}{P_{max}} \bullet \sqrt{\gamma \bullet R \bullet T_{max}} \quad (2)$$

Eng suggested using a time-based peak pressure rise rate (PPRR), as opposed to the crank angle-based rate, as a way of removing the engine speed affiliation [53,55]. A term β is used to relate PPRR, as the principal input force that drives the combustion chamber into acoustic resonance, to the largest peak-to-peak amplitude of the induced pressure oscillations. Term β was determined experimentally and is used thus: $\Delta P = \beta$.

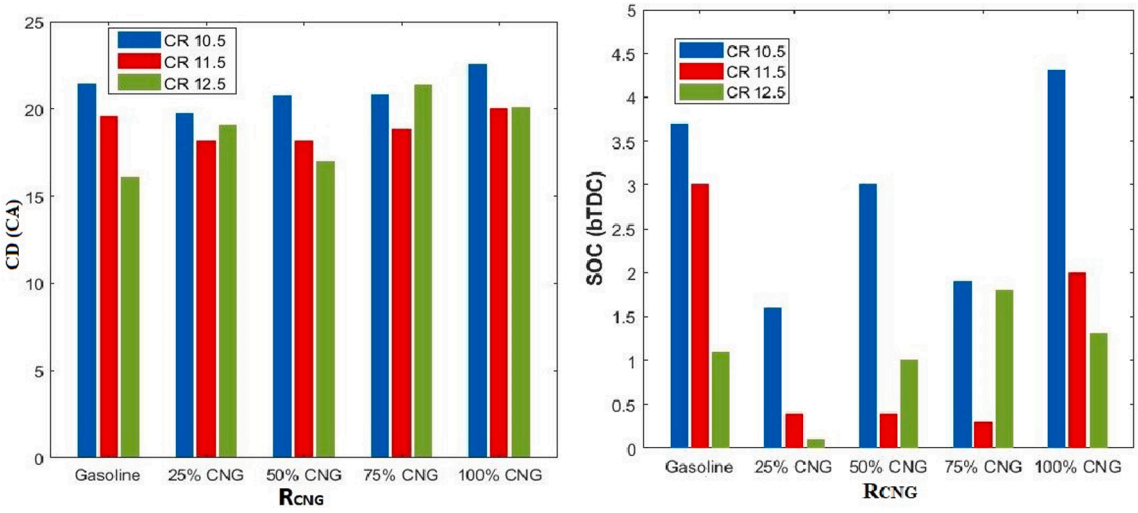

Fig. 8. Comparison of CD and SOC for various case studies.

Table 8
Combustion characteristics of various case studies under part load.

Compression Ratio	Case	SOC (CAD bTDC)	CD (CAD)	CA50 (CAD aTDC)
CR 10.5:1	Gasoline	3.7	21.40	8.74
	0.25 CNG	1.6	19.72	8.23
	0.50 CNG	3.0	20.77	7.65
	0.75 CNG	1.9	20.78	8.77
	1.00 CNG	4.3	22.57	7.69
CR 11.5:1	Gasoline	3.0	19.55	7.97
	0.25 CNG	0.4	18.14	8.25
	0.50 CNG	0.4	18.16	8.73
	0.75 CNG	0.3	18.85	8.81
	1.00 CNG	2.0	20.02	7.77
CR 12.5:1	Gasoline	1.1	16.09	8.43
	0.25 CNG	0.1	19.09	7.50
	0.50 CNG	1.0	16.98	7.95
	0.75 CNG	1.8	21.36	8.06
	1.00 CNG	1.3	20.10	7.99

Table 9
Combustion characteristics of various case studies under full load.

Compression Ratio	Case	SOC (CAD bTDC)	CD (CAD)	CA50 (CAD aTDC)
CR 10.5:1	Gasoline	3.56	15.78	6.53
	0.25 CNG	2.46	15.87	6.34
	0.50 CNG	2.51	19.93	6.6
	0.75 CNG	3.76	19.76	6
	1.00 CNG	3.45	20.3	6.89
CR 11.5:1	Gasoline	2.46	13.98	6.21
	0.25 CNG	1.99	14.19	6
	0.50 CNG	1.28	16.65	6.44
	0.75 CNG	3.4	17.88	6.03
	1.00 CNG	5.2	22.8	6.18
CR 12.5:1	Gasoline	0.48	10.33	6.43
	0.25 CNG	−0.1	12.2	7.2
	0.50 CNG	0.17	18.7	6.45
	0.75 CNG	2.99	16.89	6.66
	1.00 CNG	3.47	18.87	6

$(dp/dt)_{max}$. Maria et al. [56] expected that β should decrease considerably with peak pressure and boost level. According to other researchers, the best value for β for accurate prediction of the knock phenomenon is 0.05. Studies show that RI rises with increasing equivalence ratio and inlet temperature and decreasing CA50 [54]. In the case under study, the equivalence ratio, inlet temperature and CA50 are the same for all cases: the only variable is fuel composition. The RI value was calculated for all three CRs and all five fuel compounds, for both part- and full-load conditions (Fig. 14). As expected, RI values rise with increasing CR and they are much lower for the part load, due to the low initial pressure. Fig. 14 also shows that RI values declines with increasing R_{CNG}. Other studies have proposed different values as an acceptable upper limit of RI, the most common of which is 5 MW/m^2 [57]. However, a number of sources have put forward more cautious limits of 2 MW/m^2 and 3.5 MW/m^2 [58,59].

As illustrated in Fig. 14, none of the RI values at part load reaches even the most conservative of these limits, indicating the probability of knocking is very low. But the increase in RI in the full-load mode is considerable: the RI value exceeds all three limits when using gasoline as a pure fuel with a CR of 12.5:1, so there is a high probability of significant knocking in this mode. Raising the R_{CNG} provides a notable reduction in RI. For example, the fuel composition with just 25 % of CNG cuts RI by 56 % at full load and CR = 12.5:1. For R_{CNG} = 100 %, the RI value falls below 1 MW/m^2 at the same conditions.

Knock intensity (KI) has been used in order to validate numerical results of knock based on Kalghatgi et al. [61]. KI is defined as the difference between the maximum and minimum of the knock signal. It is determined by the evolution of the pressure wave with time following autoignition in the hot spot, that is knock onset. Bradley and colleagues [60–63], Pan et al. [64] and Bradley et al. [65] have concluded (based on the studies conducted by Zeldovich [66] and Oppenheim [67]) that the development of the pressure wave is dependent on the velocity of the autoignition wave (u_a) as it traverses through the hot spot and is given as follow:

$$u_a = \frac{\partial_x}{\partial_{\tau_i}} = \left(\frac{\partial_{\tau_i}}{\partial T}\right)^{-1}\left(\frac{\partial T}{\partial x}\right)^{-1} \tag{3}$$

Here, x is the distance from the center of the hot spot. The critical parameter ξ (resonance parameter) is the ratio of the local speed of sound, a, to u_a:

$$\xi = \left(\frac{a}{u_a}\right) \tag{4}$$

The ignition delay, τ_i, is the time taken for autoignition as marked by heat release at a given temperature and pressure [66–68,70]. An Arrhenius type equation with a pressure correction can be fitted to these kinetically derived data by ignoring larger values of τ_i (greater than 15 ms in Kalghatgi et al. [69,71]) and τ_i can be modeled by:

$$\tau_i = Aexp\left(\frac{B}{T}\right)p^{-n} \tag{5}$$

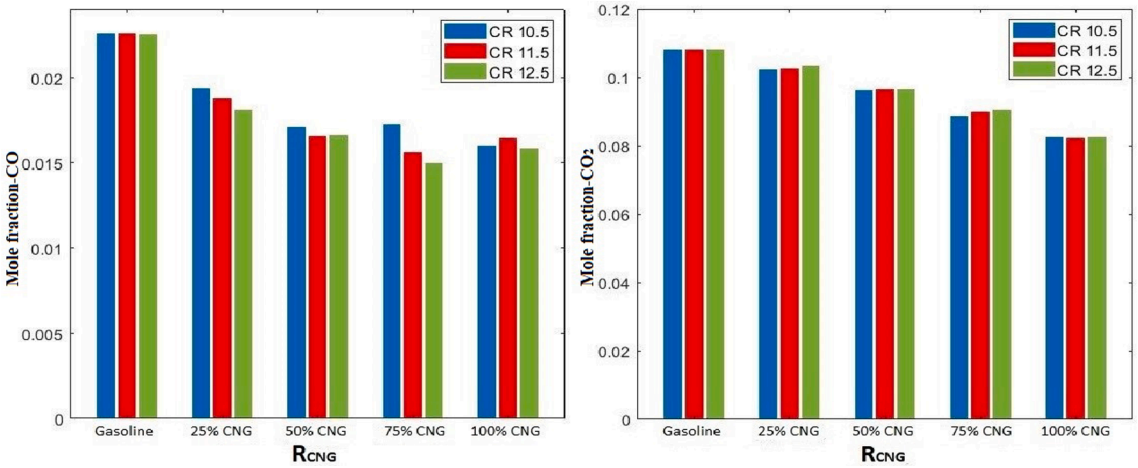

Fig. 9. Comparison of mole fraction-CO and mole fraction-CO_2 for various case studies at part load.

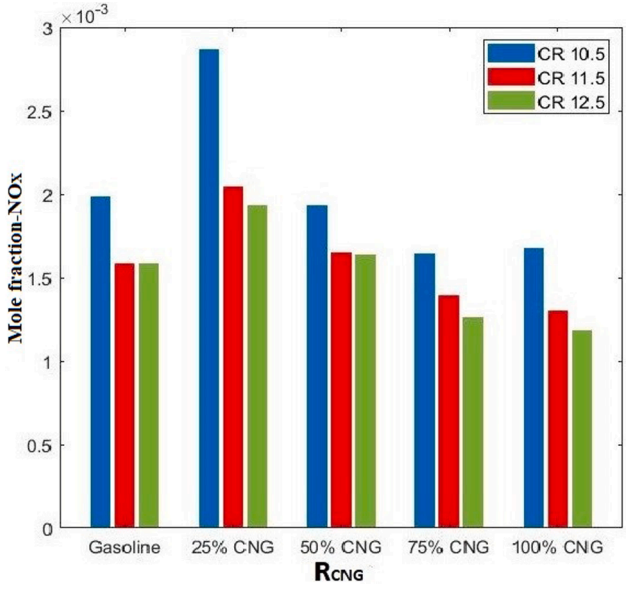

Fig. 10. Comparison of mole fraction-NOx for different cases at part load.

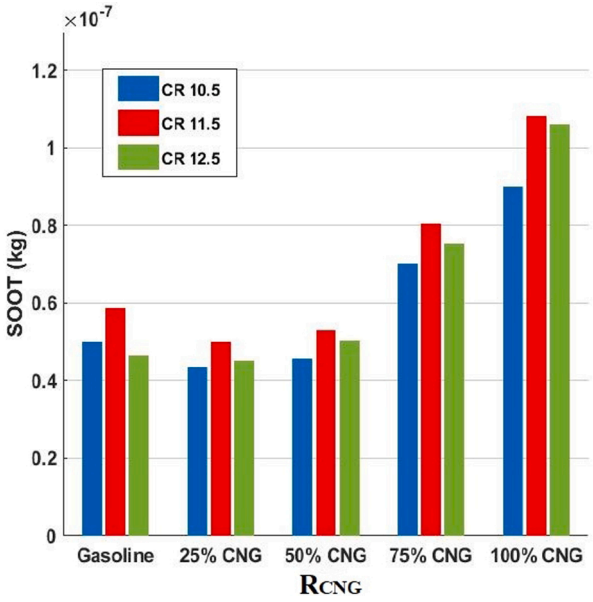

Fig. 11. Comparison of soot for various case studies at part load.

Table 10
Comparison of mole fraction-UHC for different cases under part load.

	Mole fraction-UHC ($\times 10^{-9}$) Compression Ratio		
R_{CNG}	CR = 10.5:1	CR = 11.5:1	CR = 12.5:1
0 %	2.19	2.09	8.65
25 %	752	12.2	782
50 %	8.54	3.9	263
75 %	4.34	63	15,356
100 %	40.6	12.88	8960

The speed of sound is given by:

$$a = \sqrt{\gamma RT} \tag{6}$$

where γ is the ratio of specific heats and R is the specific gas constant. A fixed value of.

375 $m^2s^{-2}K^{-1}$ for γR was assumed in Kalghatgi et al. [61]. From equation (5), the gradient of ignition delay with temperature is:

$$\left(\frac{\partial_{\tau_i}}{\partial T}\right) = -\left(\frac{B\tau_i}{T^2}\right) \tag{7}$$

Thus from equation (3):

$$u_a = -\left(\frac{T^2}{B\tau_i}\right)\left(\frac{\partial T}{\partial x}\right)^{-1} \tag{8}$$

Note that the gradient of temperature with distance in equation (8) is negative because the temperature in the hot spot is high at the center and decreases away from the center. Bradley and Kalghatgi [72] showed that when u_a is small, the maximum amplitude of the pressure pulse, ΔP_{max}, following autoignition can be approximated by:

$$\frac{\Delta P_{max}}{P} = \xi^{-2} \tag{9}$$

Also, by definition of KI, it is assumed:

$$\Delta P_{max} = \frac{KI}{2} \tag{10}$$

Hence, from equations (4), (6), (8)-(10):

$$KI = Z\left(\frac{\partial T}{\partial x}\right)^{-2} \tag{11}$$

where Z is given by:

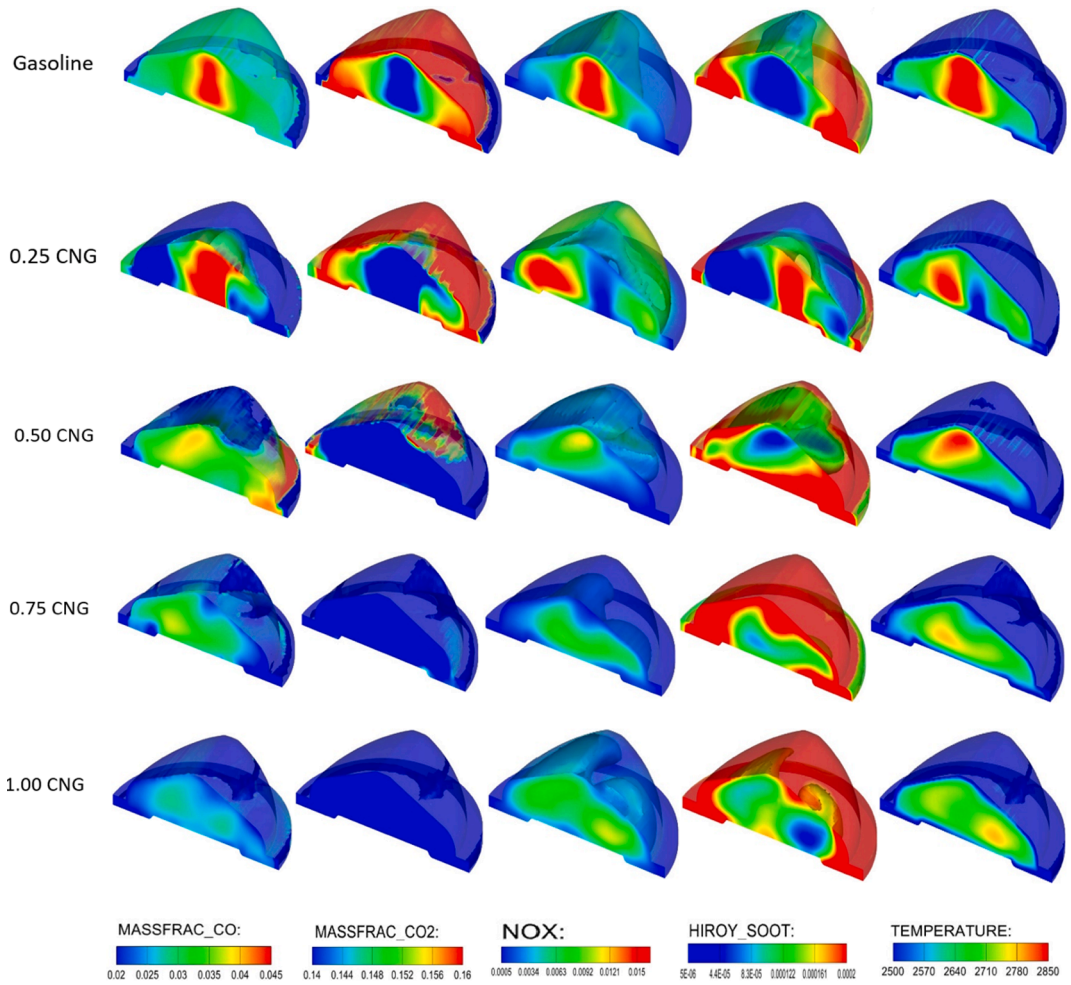

Fig. 12. Contours of CO, CO_2, NOx, Soot and temperature (18 CAD aTDC).

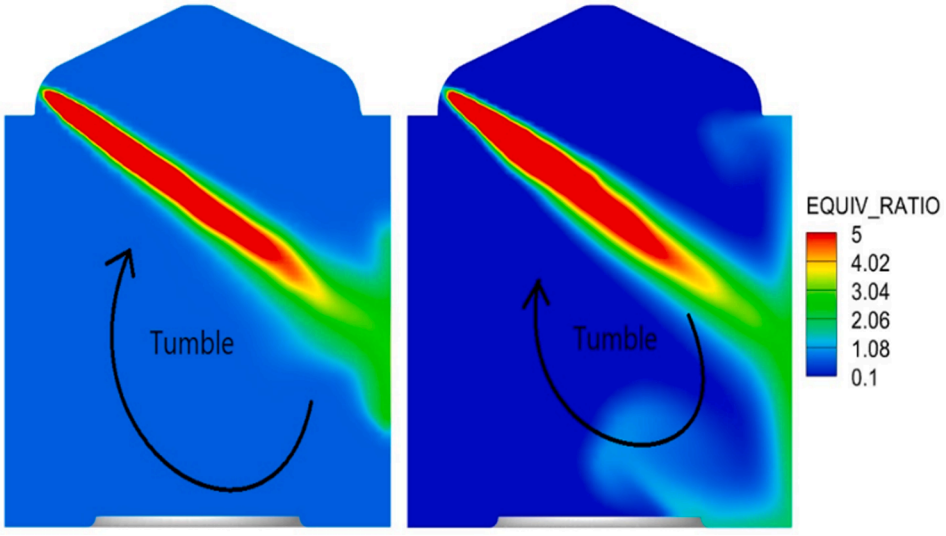

Fig. 13. Contours of equivalence ratio distribution for two modes (a) 25 % CNG; (b) 100 % CNG.

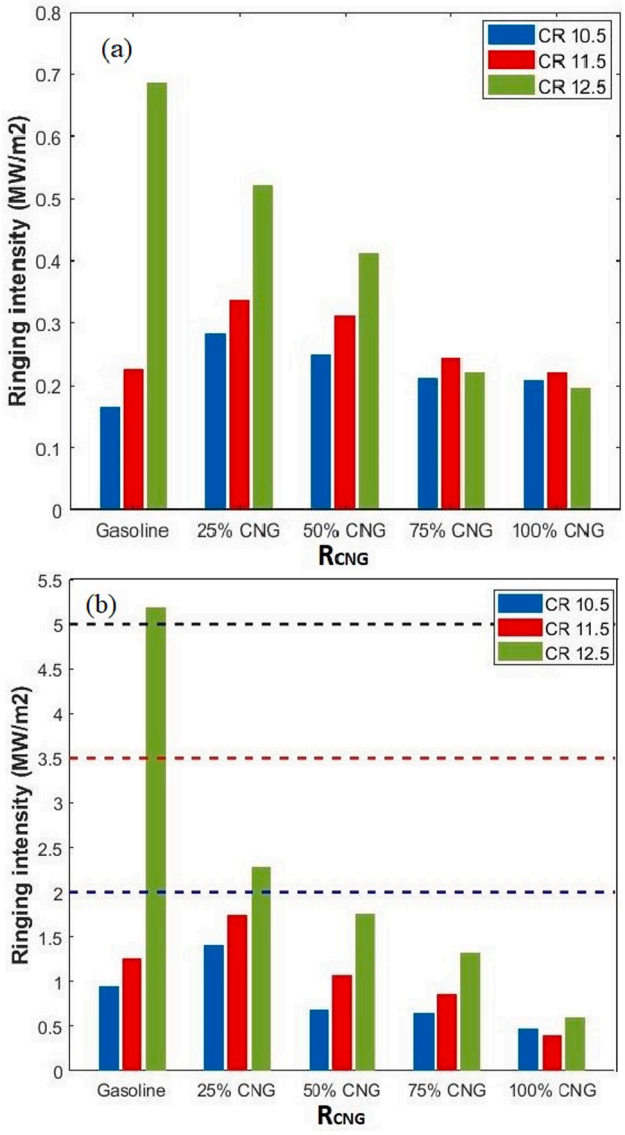

Fig. 14. Comparison of RI for various case studies (a); part load (b) full load.

$$Z = \frac{2PT^3}{375\tau_i^2 B^2} \tag{12}$$

Also.

$$\xi = -\sqrt{375T}\,\frac{B\tau_i}{T^2}\left(\frac{\partial T}{\partial x}\right) \tag{13}$$

Table 11 compares KI at CA50 ≅ 8 with the experimental value [39]. As can be seen, the numerical simulation confirms the experimental results with good accuracy. Since the temperature in Equation (13) is a function of pressure, it can be concluded that the simulation accurately predicted the in-cylinder pressure trace.

4. Conclusions

This study makes a numerical evaluation of how varying proportions of NG and different CR affect the combustion characteristics and knock behavior of a NGDI engine. Five different fuel combinations and three CRs (10.5:1, 11.5:1 and 12.5:1) are investigated at part- and full-load conditions. The main results can be summarized as follows:

Table 11
Validation of KI against measured data (CR = 10.5, WOT, R_{CNG} = 50 %).

Fuel	KI experimental data	KI simulation results
50 % CNG	0.8 bar	0.75 bar

- The fueling strategy producing the highest IMEP is for R_{CNG} = 0 %, where gasoline is homogeneously mixed with the air. With this fueling, a CR of 11.5:1 achieves the best IMEP for both part- and full-load conditions. R_{CNG} = 0 % mode also produces the highest gross work in all cases but R_{CNG} = 50 % has a higher heat release at part-load than other fuel combinations. The lowest IMEP values occurred in R_{CNG} = 100 % cases.
- At part load and with CR = 10.5:1, increasing R_{CNG} leads to higher maximum cylinder pressure: for R_{CNG} = 100 %, the maximum pressure is 5.9 % higher than with R_{CNG} = 0 %. This advantage diminishes with increasing CR. In general, the R_{CNG} = 50 % mode has the closest performance to R_{CNG} = 0 %.
- Combustion characteristics such as CA50, SOC and combustion duration is affected by changes in R_{CNG}. SOC, as measured in CAD bTDC, first is retarded by increasing the R_{CNG}, then advanced. The SOC also decreases as the CR is raised. Combustion duration shortens with increasing CR because of the consequential rise in temperature and the lower auto-ignition temperature of gasoline compared with NG. The shortest combustion duration is related to R_{CNG} = 0 % and CR = 12.5.
- Raising the CR reduces the amount of CO but causes a slight increase in CO_2. This is due to the higher combustion temperature and consequently more complete combustion. Both CO and CO_2 emissions decline with increasing R_{CNG} because NG has a lower carbon content than gasoline. For the CR ratio of 10.5:1, CO is reduced by 14.4 %, 24.7 %, 23.8 % and 29.3 % for the 25 %, 50 %, 75 % and 100 % of CNG fuels, respectively compared with pure gasoline PFI (R_{CNG} = 0 %). The corresponding reductions for CO_2 are 5.3 %, 10.8 %, 17.9 % and 23.5 %, respectively. Increasing R_{CNG} reduces NOx emissions but leads to more soot and UHC.
- RI value is low in the part-load state due to the low inlet gas pressure. The highest RI value occurs at full load when R_{CNG} = 0 % and CR = 12.5:1. The RI value rises with increasing CR but falls with increasing R_{CNG}. With a CR of 12.5:1, the RI value reduces by 56 %, 66 %, 74.6 % and 88.6 %, respectively for the 25 %, 50 %, 75 % and 100 % of CNG fuels compared with R_{CNG} = 0 %. Consequently, NGDI is very efficient for supercharged/turbocharged engines with high CRs.

CRediT authorship contribution statement

Mahdi Aghahasani: . **Ayat Gharehghani:** Supervision, Investigation. **Amin Mahmoudzadeh Andwari:** Supervision, Investigation. **Maciej Mikulski:** Supervision, Investigation. **Juho Könnö:** Supervision, Investigation.

Declaration of Competing Interest

The authors declare that they have no known competing financial interests or personal relationships that could have appeared to influence the work reported in this paper.

Data availability

Data will be made available on request.

References

[1] Reynolds CCO, Grieshop AP, Kandlikar M. Climate and health relevant emissions from in-use Indian three-wheelers fueled by natural gas and gasoline. Environ Sci Technol 2011;45(6):2406–12.

[2] A. Kakoee, A. Gharehghani, M. Mostafaei. Development of a reduced chemical kinetic mechanism for biodiesel/natural gas mixture, Fuel, 312, 2022,122920, 10.1016/j.fuel.2021.122920.

[3] Kumar A, et al. Effect of fuel injection pressure and injection timing of Karanja biodiesel blends on fuel spray, engine performance, emissions and combustion characteristics. Energy Convers Manag 2015;91:302–14. https://doi.org/10.1016/j.enconman.2014.12.004.

[4] L. Code, A Numerical Study on Effect of Ignition Timing and Mixing Ratio of Natural Gas Spark Ignition Engine on Engine Performance and Exhaust Emission Characteristics The Graduate School of the University of Ulsan Department of Mechanical Engineering Quach Nhu Y. .

[5] Liu J, Wang H. Machine learning assisted modeling of mixing timescale for LES / PDF of high-Karlovitz turbulent premixed combustion. Combust Flame 2022;238. https://doi.org/10.1016/j.combustflame.2021.111895.

[6] A. M. Andwari, A. Pesiridis, V. Esfahanian, M. F. Muhamad Said. "Combustion and Emission Enhancement of a Spark Ignition Two-Stroke Cycle Engine Utilizing Internal and External Exhaust Gas Recirculation Approach at Low-Load Operation", Energies, 2019, 12 (4), 609; 10.3390/en12040609.

[7] Agarwal AK, Singh AP, Maurya RK, Shukla PC, Dhar A, Srivastava DK. characteristics of a common rail direct injection engine using di ff erent fuel injection strategies. Int J Therm Sci 2018;134(July):475–84. https://doi.org/10.1016/j.ijthermalsci.2018.07.001.

[8] Chiong M, Kang H, Mohd N, Shaharuddin R. Challenges and opportunities of marine propulsion with alternative fuels. Renew Sustain Energy Rev 2021;vol. 149, no. May:111397. https://doi.org/10.1016/j.rser.2021.111397.

[9] A. Gharehghani, A. Kakoee, A. M. Andwari, and T. Megaritis, "Numerical Investigation of an RCCI Engine Fueled with Natural Gas / Dimethyl-Ether in Various Injection Strategies," pp. 1–25, 2021, 10.3390/en14061638.

[10] H. Xing, C. Stuart, S. Spence, and H. Chen, "Alternative fuel options for low carbon maritime transportation : Pathways to 2050," J. Clean. Prod., vol. 297, no. April 2018, p. 126651, 2021, 10.1016/j.jclepro.2021.126651.

[11] Seyam S, Dincer I, Agelin-chaab M. Novel hybrid aircraft propulsion systems using hydrogen, methane, methanol, ethanol and dimethyl ether as alternative fuels. Energy Convers Manag 2021;vol. 238, no. April:114172. https://doi.org/10.1016/j.enconman.2021.114172.

[12] Andwari AM, Said MFM, Aziz AA, Esfahanian V, Salavati-Zadeh A, Idris MA, et al. Design, Modeling and Simulation of a High-Pressure Gasoline Direct Injection (GDI) Pump for Small Engine Applications. J Mech Eng 2018;1:107–20.

[13] Karami S, Gharehghani A. Effect of nano-particles concentrations on the energy and exergy efficiency improvement of indirect-injection diesel engine. Energy Rep 2021;7:3273–85. https://doi.org/10.1016/j.egyr.2021.05.050.

[14] P.L.C. Bp, BP Statistical Review of World. Energy 2015–2017, 2017..

[15] Shi C, Zhang Z, Ji C, Li X, Di L, Wu Z. Chemosphere Potential improvement in combustion and pollutant emissions of a hydrogen-enriched rotary engine by using novel recess configuration. Chemosphere 2022;vol. 299, no. April:134491. https://doi.org/10.1016/j.chemosphere.2022.134491.

[16] D. Sankesh, J. Edsell, S. Mazlan, and P. Lappas, "Comparative study between early and late injection in a natural-gas fuelled spark-ignited direct-injection engine," vol. 110, no. December 2016, pp. 275–280, 2017, 10.1016/j.egypro.2017.03.139.

[17] M. Mikulski, J. Hunicz, K. Duda, and T. Suchocki, "Tyre pyrolytic oil fuel blends in a modern compression ignition engine : A comprehensive combustion and emissions analysis," vol. 320, no. January, 2022, 10.1016/j.fuel.2022.123869.

[18] M. M. Sławomir Wierzbicki, Kamil Duda, "Renewable Fuels for Internal Combustion Engines," https://doi.org/10.3390/en14227715.

[19] Shi C, Ji C, Wang S, Yang J, Ma Z, Ge Y. Combined influence of hydrogen direct-injection pressure and nozzle diameter on lean combustion in a spark-ignited rotary engine. Energy Convers Manag 2019;195(March):1124–37. https://doi.org/10.1016/j.enconman.2019.05.095.

[20] J. Liu and C. E. Dumitrescu, "Flame development analysis in a diesel optical engine converted to spark ignition natural gas operation," Appl. Energy, vol. 230, no. June, pp. 1205–1217, 2018, .1016/j.apenergy.2018.09.059.

[21] Liu J, Dumitrescu CE. 3D CFD simulation of a CI engine converted to SI natural gas operation using the G-equation. Fuel 2018;232(March):833–44. https://doi.org/10.1016/j.fuel.2018.05.159.

[22] H. Khatamnejad et al., "Experimental investigation on the effect of natural gas premixed ratio on combustion and emissions in an IDI engine Experimental investigation on the effect of natural gas premixed ratio on combustion and emissions in an IDI engine," J. Therm. Anal. Calorim., no. September, 2019, 10.1007/s10973-019-08726-3.

[23] Bao J, Qu P, Wang H, Zhou C, Zhang L, Shi C. Chemosphere Implementation of various bowl designs in an HPDI natural gas engine focused on performance and pollutant emissions. Chemosphere 2022;303(P3):135275. https://doi.org/10.1016/j.chemosphere.2022.135275.

[24] Shi C, Ji C, Ge Y, Wang S, Wang H, Yang J. Parametric analysis of hydrogen two-stage direct-injection on combustion characteristics, knock propensity, and emissions formation in a rotary engine. Fuel 2020;no. October:119418. https://doi.org/10.1016/j.fuel.2020.119418.

[25] Masum BM, Masjuki HH, Kalam MA, Rizwanul Fattah IM, Palash SM, Abedin MJ. Effect of ethanol-gasoline blend on NOx emission in SI engine. Renew Sustain Energy Rev 2013;24:209–22.

[26] Zhen X, Wang Y. An overview of methanol as an internal combustion engine fuel. Renew Sustain Energy Rev 2015;52:477–93.

[27] Kim J, Chun KM, Song S, Baek H-K, Lee SW. The effects of hydrogen on the combustion, performance and emissions of a turbo gasoline direct-injection engine with exhaust gas recirculation. Int J Hydrogen Energy 2017;42(39):25074–87.

[28] Sun P, Liu Ze YX, Yao C, Guo Z, Yang S. Experimental study on heat and exergy balance of a dual-fuel combined injection engine with hydrogen and gasoline. Int J Hydrogen Energy 2019;44(39):22301–15.

[29] Yu X, Guo Z, He L, Dong W, Sun P, Du Y, et al. Experimental study on lean-burn characteristics of an SI engine with hydrogen/gasoline combined injection and EGR. Int J Hydrogen Energy 2019;44(26):13988–98.

[30] "Park C, Kim C, Lee S, Lee S, Lee J. Comparative evaluation of performance and emissions of CNG engine for heavy-duty vehicles fueled with various caloric natural gases. Energy 2019;174:1–9.".

[31] Sevik J, et al. Performance, Efficiency and Emissions Assessment of Natural Gas Direct Injection compared to Gasoline and Natural Gas Port-Fuel Injection in an Automotive Engine. SAE Int J Engines 2016;9(2):1130–42. https://doi.org/10.4271/2016-01-0806.

[32] Faramawy S, Zaki T, Sakr A-A-E. Natural gas origin, composition, and processing: A review. J Nat Gas Sci Eng 2016;34:34–54.

[33] Rufford TE, Smart S, Watson GCY, Graham BF, Boxall J, Diniz da Costa JC, et al. The removal of CO2 and N-2 from natural gas: A review of conventional and emerging process technologies. J Petrol Sci Eng 2012;94–95:123–54.

[34] Liu J, Dumitrescu CE. Single and double Wiebe function combustion model for a heavy-duty diesel engine retrofitted to natural-gas spark-ignition. Appl Energy 2019;248(April):95–103. https://doi.org/10.1016/j.apenergy.2019.04.098.

[35] J. Liu and C. E. Dumitrescu, "Combustion partitioning inside a natural gas spark ignition engine with a bowl-in-piston geometry," Energy Convers. Manag., vol. 183, no. December 2018, pp. 73–83, 2019, 10.1016/j.enconman.2018.12.118.

[36] Liu J, Dumitrescu CE. Methodology to separate the two burn stages of natural-gas lean premixed- combustion inside a diesel geometry. Energy Convers Manag 2019;195(April):21–31. https://doi.org/10.1016/j.enconman.2019.04.091.

[37] Jinlong Liu CED. Numerical Investigation of Methane-Number and Wobbe-Index Effects in Lean-Burn Natural-Gas Spark-Ignition Combustion. Energy Fuels 2019. https://doi.org/10.1021/acs.energyfuels.8b04463.

[38] Cho HM, Bang-Quan H. Spark ignition natural gas engines- A review. Manag: Energy Convers; 2007.

[39] Pamminger M, Sevik J, Scarcelli R, Wallner T, Hall C. "Influence of Compression Ratio on High Load Performance and Knock Behavior for Gasoline Port-Fuel Injection. Natural Gas Direct Injection and Blended Operation in a Spark Ignition Engine" 2018. https://doi.org/10.4271/2017-01-0661.Copyright.

[40] Moradi J, Gharehghani A, Aghahasani M. Application of machine learning to optimize the combustion characteristics of RCCI engine over wide load range Application of machine learning to optimize the combustion characteristics of RCCI engine over wide load range. Fuel 2022;vol. 324, no. PA:124494. https://doi.org/10.1016/j.fuel.2022.124494.

[41] M. Pamminger, J. Sevik, S. Wooldridge, and B. Boyer, "Performance, efficiency and emissions evaluation of gasoline port-fuel injection, natural gas direct injection and blended operation," ICEF2016-9370, [Online]. Available: 10.1115/ICEF2016-9370.

[42] Mikulski M, Bekdemir C. Understanding the role of low reactivity fuel stratification in a dual fuel RCCI engine – A simulation study. Appl Energy 2017;191:689–708. https://doi.org/10.1016/j.apenergy.2017.01.080.

[43] "Jahirul MI, Masjuki HH, Saidur R, Kalam MA, Jayed MH, Wazed MA. Comparative engine performance and emission analysis of CNG and gasoline in a retrofitted car engine. Appl Therm Eng 2010;30(14-15):2219–26.".

[44] A. M. Andwari, Azhar Abdul Aziz, M .F. Muhamad Said and Z. A. Latiff, A. Ghanaati. "Influence of Hot Burned Gas Utilization on The Exhaust Emission Characteristics of A Controlled Auto-Ignition Two-Stroke Cycle Engine", International Journal of Automotive and Mechanical Eng., Vol 11 (2015), pp 2396-2404, 10.15282/ijame.11.2015.20.0201.

[45] Delpech V, Obiols J, Soleri D, Mispreuve L, Magere E, Kermarrec S. Towards an Innovative Combination of Natural Gas and Liquid Fuel Injection in Spark Ignition Engines. SAE 2018;3(2):196–209. https://doi.org/10.4271/2010-01-1513.

[46] Poorghasemi K, Saray RK, Ansari E, Irdmousa BK, Shahbakhti M, Naber JD. Effect of diesel injection strategies on natural gas/diesel RCCI combustion characteristics in a light duty diesel engine. Appl Energy 2017;199:430–46.

[47] Hiroyasu H, Kadota T. Models for Combustion and Formation of Nitric Oxide and Soot in Direct Injection Diesel Engines. SAE Trans 1976;85:513–26.

[48] Heywood, J.B., 'Internal Combustion Engine Fundamentals,' McGraw-Hill Book.

[49] Beale JC, Reitz RD. Modeling spray atomization with the Kelvin- Helmholtz/Rayleigh-Taylor hybrid model. At Sprays 1999;9:623–50.

[50] Pan S, Li X, Han W, Huang Y. An experimental investigation on multi-cylinder RCCI engine fueled with 2-butanol/diesel. Energy Convers Manag 2017;154:92–101.

[51] Liu Z, Yu X, Sun P, Xu S. Experimental investigation of the performance and emissions of a dual-injection SI engine with natural gas direct injection plus gasoline port injection under lean-burn conditions. Fuel 2021;vol. 300, no. April:120952. https://doi.org/10.1016/j.fuel.2021.120952.

[52] Husted H, Karl G, Schilling S, Weber C. Direct Injection of CNG for Driving Performance with Low CO2. 23rd Aachen Colloquium Automobile and Engine Technology. 2014.

[53] Zahdeh A, et al. Fundamental approach to investigate preignition in boosted SI engines. SAE Int J Engines 2011;4(1):246–73.

[54] Palaveev S, et al. Premature flame initiation in a turbocharged DISI engine—numerical and experimental investigations. SAE Int J Engines 2013;6(1):54–66.

[55] C. Five, "Most efficient engine," pp. 55–66, 2020.

[56] Maurya RK, Saxena MR. Characterization of ringing intensity in a hydrogen-fueled HCCI engine. Int J Hydrogen Energy 2018;43(19):9423–37. https://doi.org/10.1016/j.ijhydene.2018.03.194.

[57] Eng, J.A., Characterization of Pressure Waves in HCCI Combustion. 2002,SAE International, 10.4271/2002-01-2859.
[58] Maria, A., et al., Understanding Knock Metric for Controlled Auto-Ignition Engines. 2013,SAE International, 10.4271/2013-01-1658.
[59] J. Dernotte, J. E. Dec, and C. Ji, 'Investigation of the Sources of Combustion Noise in HCCI Engines,' 2014.
[60] J. A. E. (General M. Research), "Characterization of Pressure Waves in HCCI Combustion Reprinted From : Homogeneous Charge Compression Ignition Engines," SAE Tech. Pap. Ser., no. 724, 2018.
[61] Kalghatgi G, Algunaibet I, Morganti K. On knock intensity and superknock in SI engines. SAE Int J Engine 2017;10(3):1051–63.
[62] Ko¨nig G, Maly R, Bradley D, Lau AKC and Sheppard CGW. Role of exothermic centres on knock initiation and knock damage. SAE paper 902136, 1990.
[63] Bradley D. Autoignitions and detonations in engines and ducts. Philos T Roy Soc A 2012;370:689–714.
[64] Pan J, Sheppard C, Tindall A, Berzins M, Pennington SV and Ware JM. End gas inhomogeneity, autoignition and knock. SAE paper 982616, 1998.
[65] Bradley D, Morley C, Gu X, Emerson D. Amplified pressure waves during autoignition: relevance to CAI engines. SAE paper 2002–01-2868, 2002..
[66] Zeldovich YB. Regime classification of an exothermic reaction with nonuniform initial conditions. Combust Flame 1980;39:211–4.
[67] Oppenheim AK. Dynamic features of combustion. Philos T Roy Soc A 1985;315: 471–508.
[68] Heywood JB. Internal combustion engine fundamentals. New York: McGraw-Hill Book Co.; 1982.
[69] Kalghatgi GT. Fuel/engine interactions. Warrendale, PA: SAE International; 2014.
[70] Westbrook CK. Chemical kinetics of hydrocarbon ignition in practical combustion systems. P Combust Inst 2000;28:1563–77.
[71] Kalghatgi G, Babiker H, Badra J. A simple method to predict knock using toluene, N-heptane and iso-octane blends (TPRF) as gasoline surrogates. SAE Int J Engine 2015;8(2):505–19. SAE paper 2015–01-0757.
[72] Bradley D, Kalghatgi GT. Influence of autoignition delay time characteristics of different fuels on pressure waves and knock in reciprocating engines. Combust Flame 2009;156:2307–18.